*Journal of Sound and Vibration* (2001) **245**(1), 133–150
doi:10.1006/jsvi.2000.3545, available online at http://www.idealibrary.com on IDEAL®

# EFFICIENT MODELLING AND PREDICTION OF MESHING NOISE FROM CHAIN DRIVES

H. Zheng, Y. Y. Wang, G. R. Liu and K. Y. Lam

*Institute of High Performance Computing, Science Park I, Singapore* 118261.

and

K. P. Quek, T. Ito and Y. Noguchi

*Sunstar Engineering Inc., Kusatsu, Shiga* 525, *Japan. E-mail: zhengh@ihpc.nus.edu.sg*

(*Received* 25 *July* 2000, *and in final form* 3 *January* 2001)

This paper presents a practical approach for predicting the meshing noise due to the impact of chain rollers against the sprocket of chain drives. An acoustical model relating dynamic response of rollers and its induced sound pressure is developed based on the fact that the acoustic field is mainly created by oscillating rigid cylindrical rollers. Finite element techniques and numerical software codes are employed to model and simulate the acceleration response of each chain roller which is necessary for noise level prediction of a chain drive under varying operation conditions and different sprocket configurations. The predicted acoustic pressure levels of meshing noise are compared with the available experimental measurements. It is shown that the predictions are in reasonable agreement with the experiments and the approach enables designers to obtain required information on the noise level of a selected chain drive in a time- and cost-efficient manner.

© 2001 Academic Press

## 1. INTRODUCTION

The application of chain drives can be found extensively in nearly all mechanical industries ranging from machine tools, marine and aerospace drives to motorcycles and the timing system for automotive engines. The noise and vibration of chain drives have been of concern in the design of this kind of power transmission system. This situation should be attributed to the fact that chain drives are characterized by the discrete nature of the chain links and sprocket teeth. Undesirable noise and vibration have driven researchers to make their contributions on the dynamic behavior and vibration analyses of chain drive systems.

On the subject of vibration and noise analyses of chain drive systems, five major categories may be classified as noise source identification, load distribution analysis, kinematic analysis, dynamic and vibration analysis, and noise and vibration control [1]. Literature survey shows that, while there have been many contributions made on the topic of load analysis [2–5], kinematic analysis [6–8], and dynamics and vibration analysis [9–13], the analytical study and prediction of chain drive noise have been quite limited.

Major noise sources in roller chain drives have been identified experimentally by Uehara and Nakajima [14]. It was found that the most significant source is from the impact between the chain link and the sprocket tooth during the meshing process. This so-called

0022-460X/01/310133 + 18 $35.00/0 © 2001 Academic Press

"meshing noise" is closely related to the overall dynamic behavior of the chain and various parameters. A further experiment conducted by Stone *et al.* [15] also showed that the noise level and the impact during engagement are closely correlated. Liu *et al.* [16] presented a comprehensive analysis of the chain/sprocket impact dynamics with analytical models including an axially moving chain dynamic model and a chain drive system dynamic model. Through experimental investigations, they illustrated a direct relationship between the chain/sprocket meshing impulsive loads and the nearfield sound pressure levels. To the best of the authors' knowledge, a semi-empirical formula given by Uehara and Nakajima [14] is so far the only one which may be used for the estimation of sound level of the meshing noise from chain drives. Before their formula can be used to estimate the noise radiation from a roller chain drive, several constants ($C_5$ and $C_6$ of equations (12) and (13) in reference [14]) required for acoustic energy calculation must be determined through experimental measurements on similar chain drives.

The boundary element method (BEM) has long been an effective numerical technique for the calculation of the acoustic radiation problem [17, 18]. The main advantage of BEM is the reduction of the structural discretization and data preparation time which results from the reduction of the dimensionality of the problem by one. However, BEM suffers from some shortcomings including evaluation of singular terms and handling the non-uniqueness of the solutions. Furthermore, owing to the limitations of data transfer interface between existing commercial software codes for structural analysis using finite element method (FEM) and those for acoustic radiation analysis using BEM, there still exist some difficulties in directly utilizing combined FEM/BEM to simulate the meshing noise from such a complicated mechanical system as a chain drive comprising a large number of discrete elements.

Presented in this paper is a pratical approach for the noise level prediction of a roller chain drive. The approach divides the task of chain drive noise prediction into two steps. First, an acoustical model relating the dynamic response of rollers and its induced sound pressure is developed on the basis of the fact that the acoustic field is mainly created by oscillating rigid cylindrical rollers, and the numerical procedure for the noise level prediction of a roller chain drive is programmed on the basis of an acoustical model. Second, finite element modelling and simulation techniques are applied to analyze the impact responses of both the chain roller and sprocket. The simulation results of impact accelerations are read as input data in the developed software program for the calculation of the sound pressure at arbitrary points of observations.

One merit of the presented approach is that it enables a designer to obtain his required information on the noise level of a chain drive in an efficient manner. Furthermore, since there are a number of commercially available computer-aided engineering (CAE) tools which can be employed for dynamics analysis of roller chain drives, the numerical procedure developed for calculating the noise level from a roller chain drive can be readily integrated into an existing CAE environment to create a complete virtual acoustical simulation capability for chain drive system design.

## 2. ACOUSTICAL MODEL

### 2.1. REVIEW OF MESHING NOISE CREATING MECHANISM

It has been identified that the meshing noise, which is caused by the interaction between the sprocket teeth and the chain rollers during their engagements, is the first and most significant noise source in the roller chain drives [14]. The polygonal action and the

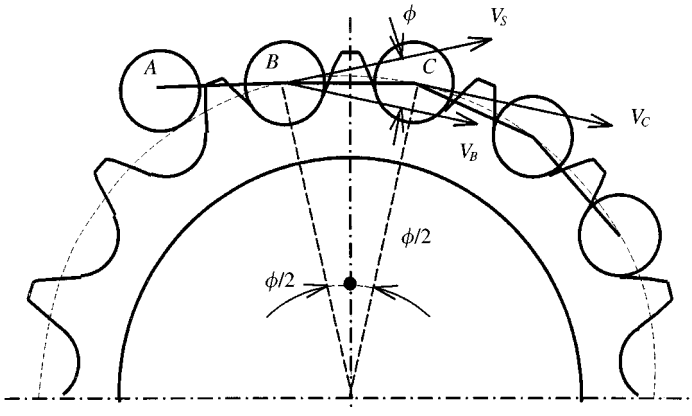


Figure 1. Impact velocity of chain rollers.

roller–sprocket impact, being intrinsic for roller chain drives, are responsible for the meshing noise creating mechanism.

Figure 1 depicts the position of the chain and sprocket at an infinitesimal time depicted before roller A is seated. The relative impact velocity of the roller is the velocity between the center of the roller and the point on the sprocket pitch circle which will be coincident with the roller center after seating [19], namely,

$$V_R = V_S \sin(\varphi/2) + V_A \sin(\varphi/2), \tag{1}$$

where $V_A$ and $V_S$ are the roller velocity before and after seating, respectively,

$$V_A = V_C = 2\pi Rn/60, \qquad V_S = 2\pi Rn/60, \tag{2, 3}$$

where $R$ is the sprocket pitch circle radius and $n$ is the rotational speed of the sprocket in r.p.m.

Although the magnitudes of the velocities $V_A$ and $V_S$ are the same, the directions are different. So the relative impact velocity of the roller is

$$V_{impact} = 2\pi Pn/60, \tag{4}$$

where $P$ is the link pitch.

This indicates that there exists a very big relative impact velocity at an infinitesimal time when a roller is picked up by the sprocket teeth. The relative impact velocity of the roller onto the sprocket teeth causes the roller and sprocket to vibrate with elastic vibrations and a large rigid acceleration of the impacting roller, of which the latter in turn causes a sudden change of the pressure of the air around the impact area. So the calculation of sound energy of the meshing noise generated by a chain drive system should consider the contributions of both rollers and sprockets as

$$E = \sum_{i=1}^{N_1} E_{i,sprkt} + \sum_{i=1}^{N_2} E_{i,roller}, \tag{5}$$

where $N_1$ and $N_2$ are, respectively, the number of sprockets and chain rollers. Through a large amount of detailed modelling of the impact between roller and sprocket and detailed experimental measurements on noise radiation from concerned chain drives [20], we found

that, during the very short period when a roller is picked by the sprocket, the elastic vibration response of the sprocket and further induced noise level are much lower than those due to the vibration of rollers. So it is fair to neglect the contribution of the sprockets in developing the acoustical model for noise level prediction.

## 2.2. THEORY

The chain rollers that are engaging successively with the sprocket teeth may be modelled as a series of oscillating cylinders. The acoustic equation for the cylinder in a cylindrical co-ordinate system $r$, $\theta$ and $Z$ as shown in Figure 2 is given by [21]

$$\frac{1}{r}\frac{\partial}{\partial r}\left(\frac{1}{r}\frac{\partial \Phi}{\partial r}\right)+\frac{1}{r^2}\frac{\partial^2 \Phi}{\partial \theta^2}+\frac{\partial^2 \Phi}{\partial Z^2}=\frac{1}{C}\frac{\partial^2 \Phi}{\partial t^2}, \tag{6}$$

where $\Phi$ is the velocity potential, $C$ is the sound speed in the air, $t$ is time. The sound pressure, $p$, the particle velocity, $U_r$, are determined by the relation

$$p=\rho_0\frac{\partial \Phi}{\partial t}, \qquad U_r=-\frac{\partial \Phi}{\partial r}. \tag{7}$$

If the oscillating cylinder vibrates with a velocity of $v_0 e^{j\omega t}$, the velocity potential $\Phi(r, \theta, t)$ becomes

$$\Phi(r, \theta, t)=A\cos\theta H_1^{(2)}(kr)e^{j\omega t}, \tag{8}$$

where $H_1^{(2)}(kr)$ is the second kind Hankel function (first order), $\omega$ is the angular frequency of oscillation and $k$ is equal to $\omega/C$. If the plane of vibration is taken as the reference plane, the angle between the velocity of the cylinder surface and the plane of vibration is $\theta$, then with the boundary condition

$$U_r|_{r=a}=-\left.\frac{\partial \Phi}{\partial r}\right|_{r=a}=v_0 e^{j\omega t}\cos\theta, \tag{9}$$

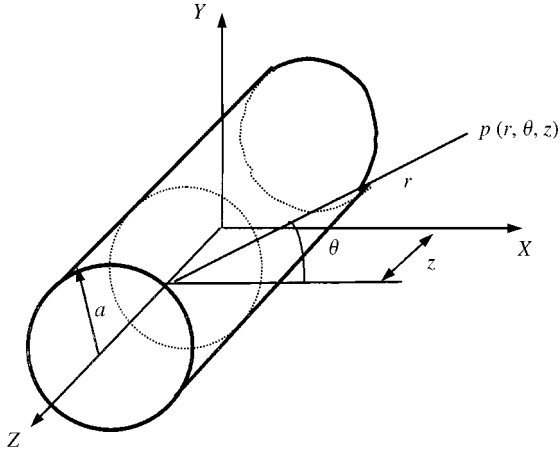


Figure 2. Cylindrical co-ordinate system.

where $a$ is the radius of the cylinder. Coefficient $A$ in equation (8) can be therefore obtained as

$$A = -\frac{v_0}{kH_1^{(2)\prime}(ka)}, \tag{10}$$

where $H_1^{(2)\prime}(ka)$ is the differentiation of $H_1^{(2)}(kr)$ with respect to $kr$ at $r = a$. Substituting $A$ into equation (8), the velocity potential is obtained as

$$\Phi(r, \theta, t) = -v_0 \cos\theta \frac{H_1^{(2)}(kr)}{kH_1^{(2)\prime}(ka)} e^{j\omega t}. \tag{11}$$

The velocity potential for any arbitrary velocity of the oscillating cylinder can be obtained by Fourier synthesis of this solution when the Fourier transform of the velocity is known. The velocity potential for an arbitrary $v_0(\omega)$ is

$$\Phi(r, \theta, t) = -\frac{\cos\theta}{2\pi} \int_{-\infty}^{\infty} \frac{v_0(\omega) H_1^{(2)}(kr) e^{j\omega t}}{kH_1^{(2)\prime}(ka)} d\omega. \tag{12}$$

If the velocity of the cylinder is due to a unit impulse of acceleration, then its transform is

$$v_0(\omega) = B\delta(\omega) + \frac{1}{j\omega}, \tag{13}$$

where $B$ is an arbitrary constant and $\delta(\omega)$ is the Delta function. The velocity potential due to a unit impulsive acceleration then becomes

$$I(r, \theta, t) = -\frac{\cos\theta}{2\pi} \int_{-\infty}^{\infty} \frac{B\delta(\omega) + 1/j\omega}{kH_1^{(2)\prime}(ka)} H_1^{(2)}(kr) e^{j\omega t} d\omega. \tag{14}$$

Using the expression $k = \omega/C$, the velocity potential from the acceleration, $a(t)$, of the oscillating cylinder is

$$\Phi(r, \theta, t) = \int_0^t I(r, \theta, t' - \tau) a(\tau) d\tau,$$

$$= -\frac{\cos\theta}{2\pi} \int_0^t \int_{-\infty}^{\infty} a(\tau) \frac{B\delta(\omega) + 1/j\omega}{(\omega/c) H_1^{(2)\prime}(a\omega/c)} H_1^{(2)}\left(\frac{r\omega}{c}\right) e^{j\omega(t' - \tau)} d\omega\, d\tau. \tag{15}$$

The Hankel function is the third kind Bessel function. As given in reference [22] (see pp. 358–389), the asymptotic expansion of the second kind Hankel function is a simple expression given as

$$H_v^{(2)}(x) = \left(\frac{2}{\pi x}\right)^{1/2} \exp^{-j(x - v\pi/2 - \pi/4)} \left[1 + \sum_{n=1}^{\infty} \frac{(v, n)}{(2jx)^n}\right], \tag{16}$$

where $(v, n)$ is a symbol which is defined as

$$(v, 0) = 1,$$

$$(v, n) = (-1)^n \frac{(\frac{1}{2} - v)_n (\frac{1}{2} + v)_n}{n!} = \frac{[4v^2 - 1][4v^2 - 3^2] \cdots [4v^2 - (2n - 1)^2]}{2^{2n} n!},$$

where $v = 0, 1, 2$ are, respectively, for the zero, first and second order Hankel functions.

The values of $(v, n)$ when $n$ equals 1 and 2 are calculated, respectively, as

$$(0, 1) = -1/4, \quad (0, 2) = 9/32, \quad (1, 1) = 3/4, \quad (1, 2) = -15/32,$$

$$(2, 1) = 15/4, \quad (2, 2) = 105/32.$$

Provided that the variable $x$ is not very small, equation (16) can be approximated as

$$\mathrm{H}_v^{(2)}(x) = \left(\frac{2}{\pi x}\right)^{1/2} \exp^{-\mathrm{j}(x - v\pi/2 - \pi/4)} \left[1 + \frac{(v, 1)}{2\mathrm{j}x} + \frac{(v, 2)}{(2\mathrm{j}x)^2}\right] \tag{17}$$

with neglecting other terms for $n \geqslant 3$ inside parentheses. This simplification does not significantly deteriorate the accuracy of calculating the velocity potential of the sound field, especially for a far field.

So the first order Hankel function of the second kind can be expressed as

$$\mathrm{H}_1^{(2)}(x) = \left(\frac{2}{\pi x}\right)^{1/2} \mathrm{e}^{-\mathrm{j}(x - 3\pi/4)} \left[1 + \frac{3}{8\mathrm{j}x} + \frac{15}{128x^2}\right]. \tag{18}$$

According to the recurrence relation of all kinds of Bessel functions, the derivative of the the first order Hankel function of the second kind is related to its zero and second orders as

$$\mathrm{H}_1^{(2)\prime}(x) = \frac{1}{2}\left[\mathrm{H}_0^{(2)}(x) - \mathrm{H}_2^{(2)}(x)\right], \tag{19}$$

where $\mathrm{H}_0^{(2)}(x)$ and $\mathrm{H}_2^{(2)}(x)$ are, respectively, the zero and the second order Hankel functions of the second kind,

$$\mathrm{H}_0^{(2)}(x) = \left(\frac{2}{\pi x}\right)^{1/2} \mathrm{e}^{-\mathrm{j}(x - \pi/4)} \left[1 - \frac{1}{8\mathrm{j}x} - \frac{9}{128x^2}\right], \tag{20}$$

$$\mathrm{H}_2^{(2)}(x) = -\left(\frac{2}{\pi x}\right)^{1/2} \mathrm{e}^{-\mathrm{j}(x - \pi/4)} \left[1 + \frac{15}{8\mathrm{j}x} - \frac{105}{128x^2}\right]. \tag{21}$$

So the derivative of $\mathrm{H}_1^{(2)}(x)$ is

$$\mathrm{H}_1^{(2)\prime}(x) = \left(\frac{2}{\pi x}\right)^{1/2} \mathrm{e}^{-\mathrm{j}(x - \pi/4)} \left[1 + \frac{7}{8\mathrm{j}x} - \frac{57}{128x^2}\right]. \tag{22}$$

Substituting $kr$ and $ka$ for $x$ into equations (19) and (20), respectively, equation (14) becomes

$$I(r, \theta, t) = -\frac{\cos\theta}{2\pi} \mathrm{j}C \sqrt{\frac{a}{r}} \int_{-\infty}^{\infty} \left[B\delta(\omega) + \frac{1}{\mathrm{j}\omega}\right] \frac{(1 + 3C/8\mathrm{j}\omega r)\mathrm{e}^{\mathrm{j}\omega(t - (r - R)/C)}}{\omega[1 + 7/8\mathrm{j}\omega a + 57/128(\mathrm{j}\omega a)^2]} \mathrm{d}\omega. \tag{23}$$

This equation is evaluated by contour integration in the complex plan. By solving the equation

$$\left[1 + \frac{7}{8\mathrm{j}\omega\omega} + \frac{57}{128\,\mathrm{j}\omega\mathrm{j}\omega^2}\right] \frac{1}{\omega^2} = 0 \tag{24}$$

three singularities of the function to be integrated are attained as

$$\omega_1 = 0, \qquad \omega_2 = l_1 + \mathrm{j}l_2, \qquad \omega_3 = -l_1 + \mathrm{j}l_2,$$

where

$$l_1 = \frac{\sqrt{65}C}{16a}, \qquad l_1 = \frac{7C}{16a}.$$

Correlative residuals are derived to obtain the solution of equation (23) as

$$I(r, \theta, t) = \sqrt{\frac{a}{r}} \cos\theta \frac{16}{\sqrt{65}} a \left\{ \mathrm{e}^{-l_2(t(r-a)/C)} \left[ \left(1 - \frac{7}{19}\frac{a}{r}\right) \sin l_1 \left(t - \frac{r-a}{C}\right) - \frac{\sqrt{65}}{19} \cos l_1 \left(t - \frac{r-a}{C}\right) \right] + \frac{\sqrt{65}}{19}\frac{a}{r} \right\}. \tag{25}$$

This equation is quite similar in format to the one derived by Wang and Tong in reference [23], where they use it to predict the noise radiation from the impact of two cylinders, but of difference are the coefficient before the flower bracket and those for sine and cosine terms.

From the above derived equation, one can see that the near sound field is radiated in a complex manner by an impact cylinder. However, for the far sound field, i.e., $r \gg a$, equation (25) can be simplified as

$$I(r, \theta, t) = \sqrt{\frac{a}{r}} \cos\theta \frac{16}{\sqrt{65}} a \sin l_1 \left(t - \frac{r-a}{C}\right) \mathrm{e}^{-\mathrm{j}l_2(t-(r-a)/C)}. \tag{26}$$

Similarly, the solution of equation (15) is

$$\Phi(r, \theta, t) = \sqrt{\frac{a}{r}} \cos\theta \frac{16}{\sqrt{65}} a \int_0^t a(\tau) \sin l_1 \left(t - \frac{r-a}{C} - \tau\right) \mathrm{e}^{-\mathrm{j}l_2(t-(r-a)/C-\tau)} \mathrm{d}\tau. \tag{27}$$

The sound pressure at point $P(r, \theta)$ caused by the impact acceleration of a roller is given by

$$p(r, \theta, t) = \rho_0 \frac{\partial \Phi(r, \theta, t)}{\partial t}, \tag{28}$$

where $\rho_0$ is the density of the air medium, $\rho_0 = 1{\cdot}2\ \mathrm{kg/m^3}$.

As the impact of the roller against the sprocket occurs in a very short duration, it is reasonable to consider each roller independent of the others. So the total sound pressure radiated by the acceleration of all impacting rollers is taken simply as the sum of those from the rollers separately, i.e.,

$$p(r, \theta, t) = \sum_i p_i(r_i, \theta_i, t) \quad (i = 1, 2, \ldots, N_2). \tag{29}$$

### 2.3. NUMERICAL IMPLEMENTATION AND PROGRAMMING

For the purpose of numerical programming, the above-derived equations are written in the format of both numerical integration and differentiation. On the other hand, the simulation results of acceleration of impact rollers are outputed in a format of discrete data

in time domain, which also requires a numerical implementation of integration and differentiation for sound pressure calculation.

The time domain is first divided into a series of small sub-domains with a constant time interval $\Delta t$. At a discrete time $t_j$, the velocity potential generated by a acceleration of the roller $i$ given by equation (27) can be approximated by

$$\phi_{ij}(r_{ij}, \theta_{ij}, t_j) = \sum_{j_i=1}^{t_j} I_{ij_1}(r_{ij_1}, \theta_{ij_1}, t_j - \tau_{j_1}) A_i(\tau_{j_1}) \Delta\tau. \tag{30}$$

Similarly, the velocity potential generated by the acceleration of all rollers in the two considered directions and the total velocity potential can also be written as

$$\phi_{xj}(r_{xj}, \theta_{xj}, t_j) = \sum_{i=1}^{N} \phi_{xij}(r_{xij}, \theta_{xij}, t_j), \tag{31a}$$

$$\phi_{yj}(r_{yj}, \theta_{yj}, t_j) = \sum_{i=1}^{N} \phi_{yij}(r_{yij}, \theta_{yij}, t_j), \tag{31b}$$

$$\phi_j(r_j, \theta_j, t_j) = \phi_{xj}(r_{xj}, \theta_j, t_j) + \phi_{yj}(r_{yj}, \theta_{yj}, t_j). \tag{32}$$

And finally, the sound pressure at point $p(r, \theta)$ can be approximated by

$$p(r, \theta, t_j) = \rho_0 \frac{\phi_j(r_j, \theta_j, t_j) - \phi_{j-1}(r_{j-1}, \theta_{j-1}, t_{j-1})}{t_j - t_{j-1}}. \tag{33}$$

The time history of the sound pressure of the roller chain drive is therefore attained through the summation of acceleration noise pressure, respectively, due to each impact of the engaging roller with the sprocket tooth. The noise level in dB of the system at an observed point, $x$ or in cylindrical co-ordinate system $(r, \theta)$, is calculated as

$$\begin{aligned} L_p &= 10 \lg \left( \frac{p_{r.m.s.}^2}{p_{ref}^2} \right) \\ &= 10 \lg \left[ \frac{1}{T} \int_0^T \frac{p^2(t)\,\mathrm{d}t}{(2 \times 10^{-5})^2} \right] \\ &= 10 \lg \left[ \frac{1}{T} \sum_{t_j=1}^{t_j=T} \frac{p^2(r, \theta, t_j)\Delta t}{(2 \times 10^{-5})^2} \right], \end{aligned} \tag{34}$$

where $T$ is the time window for integration.

This numerical procedure for the calculation of both sound pressure and noise level is implemented through programming using FORTRAN77. The program consists of four parts, i.e., acoustic parameter definition and reading-in of the finite element analyzed acceleration time history of rollers, calculation of sound pressure time history for all designated points on a hypothetical surface, noise level through integration in time-domain, the Fourier transform of sound pressure to frequency domain, and, if required, the calculation of sound power of the whole system.

The acoustic parameters of the medium and the co-ordinates of all designated points are specified first. The time history of the acceleration in the two directions and the co-ordinates of each roller impact against the sprocket tooth successively are read in by the program. Both polar angles, $\theta_x$ and $\theta_y$, and the distance, $r_x$ and $r_y$, from the designated point to the

center of the roller under consideration are thus calculated. The velocity potentials generated by the acceleration of the roller under consideration in two directions are then obtained. These velocity potentials are summed for all rollers and for two directions to obtain the velocity potential generated by the whole system, which is furthermore used to calculate the sound pressure through numerical differentiation given by equation (33).

The outputs of the program include a data file for writing the sound pressure level at each designated point and the sound power level in dB, and a series of data files containing the sound pressure time history of these points.

## 3. FINITE ELEMENT MODELLING OF CHAIN ROLLER RESPONSE

In order to achieve a reliable prediction of the noise level, it is crucial to attain an accurate solution of the impact responses of the impacting rollers. On the dynamics and vibration analysis of roller chain drive systems, there exist a lot of analytical models which may be used for the calculations of chain rollers' velocity, even impulsive loads or contact strength between roller and sprocket and vibration of chain span [10–13, 16]. Owing to the complexity of the problem; however, these analytical models have seldom taken into account such important aspects of dynamic roller drives as the elasticity of the roller and sprocket in high operation speed, the clearances between the bush and pin as between the roller and bush as well, etc. This situation leads us to consider employing finite element modelling and simulation techniques to simulate the impact response of the engaging rollers instead of using the existing analytical model.

The numerical investigation is limited to the case of a chain–sprocket system running at constant speeds and driving torque. Focuses are on the impact of roller assemblies against the sprocket and the induced dynamic response of chain rollers.

The finite element model of a typical two-sprocket chain drive for the power transmission of a motorcycle is shown in Figure 3. This chain drive comprises 110 chain link assemblies, a 15-tooth drive sprocket, and a 42-tooth driven sprocket. Each chain link assembly in this model further comprises a cylindrical roller, a bush, a pin and two link plates. Both sprockets and all chain links are modelled in full geometrical details. Eight-node brick elements are used to construct the finite element model of sprockets, rollers and bearing

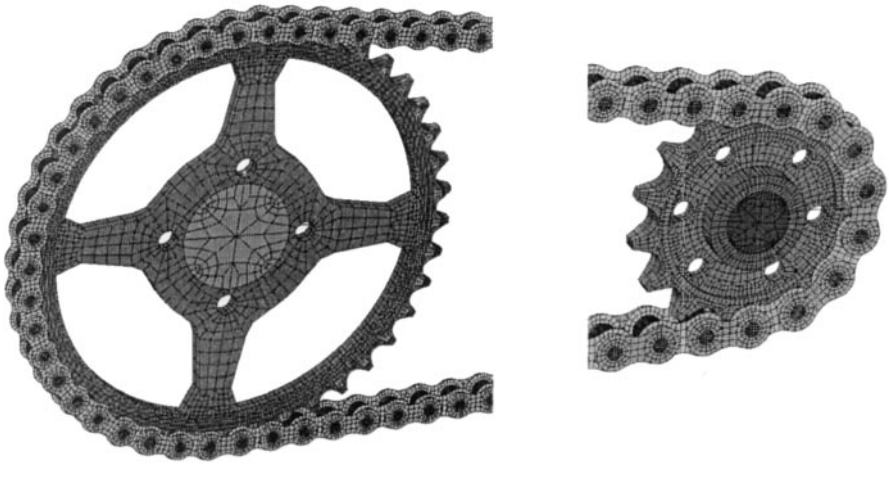

Figure 3. Finite element model of roller chain drive.

TABLE 1

*Geometry of two sprocket*

| Dimension (mm) | Drive sprocket | Driven sprocket |
|---|---|---|
| Outside diameter | 81·8 | 219·0 |
| Pitch diameter | 76·85 | 212·43 |
| Bottom diameter | 66·28 | 202·82 |
| Hub diameter | 33·0 | N.A. |
| Bore | 25·0 | N.A. |
| Pitch | 15·875 | |

TABLE 2

*Dimension of the chain roller components*

| Component | Inner diameter (mm) | Outer diameter (mm) | Cylinder length (mm) |
|---|---|---|---|
| Roller | 7·52 | 10·20 | 7·0 |
| Bushing | 5·33 | 7·43 | 9·94 |
| Pin | 2·68 | 5·24 | 14·94 |

TABLE 3

*Physical parameters of material*

| Young's modulus ($kN/mm^2$) | Shear modulus ($kN/mm^2$) | The Poisson ratio | Density ($kg/mm^3$) |
|---|---|---|---|
| 210 | 85 | 0·28 | 7·86E-6 |

pins, while the link plates, and bushes are meshed using 2-D shell elements. The whole model consists of 78 744 solid elements, 33 440 shell elements, and 171 245 nodes. Tables 1 and 2 list the major geometrical parameters of two sprockets and chain links of the model respectively.

All the components except the bushes between the respective roller and bearing pin are modelled as rigid bodies to simplify the modelling process and to attain the required information for noise calculation in a time-efficient manner. The physical parameters of the steel material for all the components are given in Table 3.

A total of 272 contact interfaces are defined between all components potentially in contact with each other in the model such as among roller–bush, bush–pin, and particularly the physical engagement between the roller–sprocket to the model. A penalty method is adapted to surface–surface contact algorithm for possible penetration search. To take account of the shell thickness, stiffness of the material and the friction between two contacting surfaces into the contact calculation scheme, appropriate penalty parameters are defined to ensure a smooth engagement of the rollers with the sprockets. A maximum search frequency, i.e., one search per time step, is selected to ensure sufficient analysis accuracy.

Modelling of the power supply and power consumption is one of the most difficult aspects of the analysis of dynamic systems. Since our numerical simulation is limited to the case of the chain–sprocket system running at a constant speed, a fixed rotational velocity of 0·12074 rad/ms, which represents a motor speed of 50 km/h, is applied to the drive sprocket. Meanwhile, a constant resisting torque is applied on the driven sprocket representing a driven torque of 150 N m. The other specified FE entities include displacement boundary conditions of two sprocket centers, gravity of all components.

A commercial software for explicit finite element analyses of non-linear dynamic problems is employed for the calculation of dynamic response of both rollers and sprockets in time domain under specified loading and boundary conditions. The termination time input for one dynamic run is as long as 30 ms, about 9 times the time for a roller to move in one pitch distance. The selected nodes on the rollers and interested locations of the two sprockets are specified to output the displacements, velocities and accelerations. The results from the software code include both a visualization of the behavior of the system and the numerical results. All these numerical solutions of the acceleration of each roller will be the input data of the present program for noise calculation.

As a few examples, Figure 4 depicts the velocity time history of a chain roller around it is seated onto a drive sprocket tooth, together with the contact force between the roller and sprocket tooth represented by a solid line. It can be seen that the velocity of the moving roller changes significantly in its impact direction ($Y$-axis) at an infinitesimal time it seats on the sprocket tooth. This impact is the dominant mechanism of chain drive noise. Figure 5

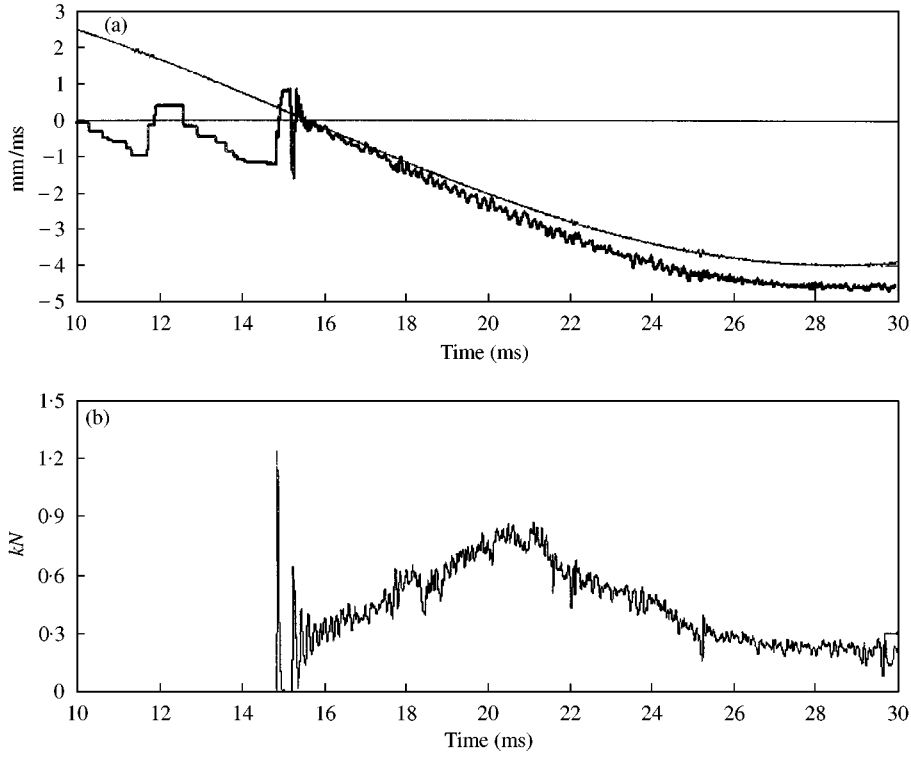


Figure 4. Comparison of velocity of chain roller and tooth of drive sprocket together with the relationship between the velocity of roller and the contact force. (a) ——, Velocity_y (tooth bottom); ———, velocity_y (roller). (b) ——, Contact_Force_2.

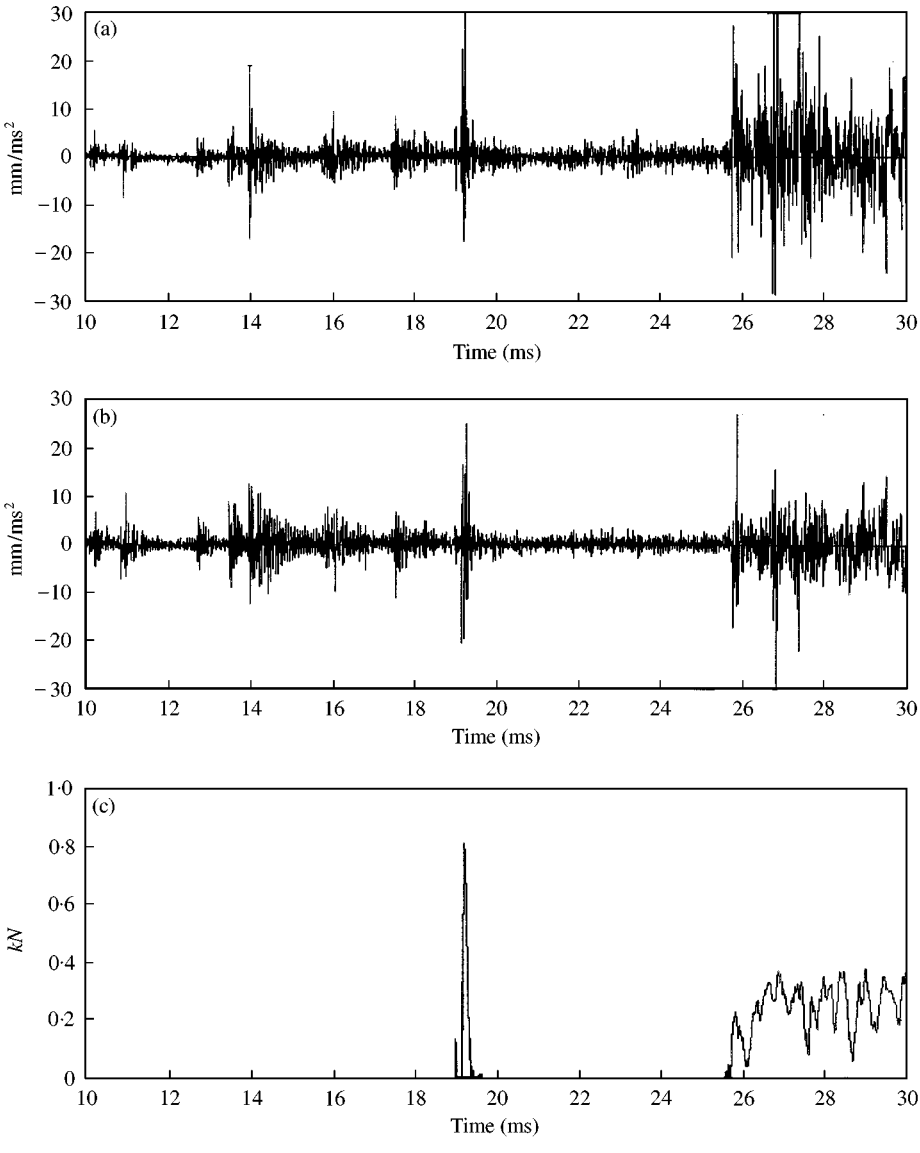


Figure 5. Acceleration of chain roller and the contact force between the roller and the tooth of driven sprocket. (a) ——, acceleration_x; (b) ——, acceleration_y; (c) ——, Contact_Force.

shows the acceleration of the roller in the $X$ and $Y$ directions, together with the contact force between the roller and a tooth of the driven sprocket. Figure 6 gives the acceleration and the contact force for the roller engaging with the drive sprocket. Comparing these figures, one can find that the acceleration response of the roller in the $Y$ direction is strongly correlated with the contact force between the roller and sprocket which also represents the intensity of the impact. The magnitude of roller acceleration is different from one roller to another due to the transverse vibration of both tight and slack chain spans. Due to the lower rotational speed of the driven (big) sprocket and the slackness of the chain strand on the slack side, the impact between chain rollers with the driven sprocket is much weaker than that between rollers with the drive sprocket. This is illustrated in Figure 7 where

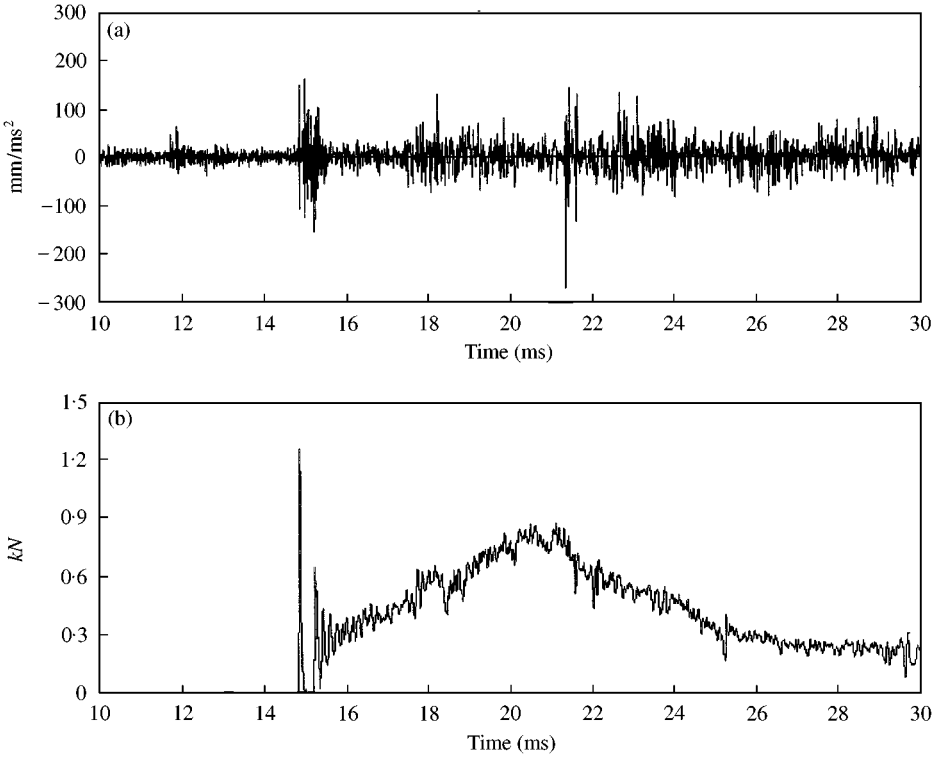


Figure 6. Acceleration of chain roller in $Y$ direction and the contact force between the roller and the tooth of drive sprocket. (a) ——, acceleration_y; (b) ——, Contact_Force_2.

a comparison of typical time histories of contact force between four successive chain rollers with drive sprocket teeth is shown.

## 4. NOISE LEVEL PREDICTION AND COMPARISON WITH MEASUREMENTS

The noise level prediction results of the chain drive at different observed points are compared with the experimental measurements. The measurement is conducted in a 1·78 m × 2 m × 1·78 m semi-anechoic room with one reflecting plane which is parallel with the chain drive plane. Details of this room and used driving as well as the loading system for the testing can be seen in reference [24]. According to the International Organization for Standardization (ISO), a hypothetical hemisphere or a rectangular parallelpiped surface is normally selected for surrounding the machine to measure the sound pressure at respective locations [25]. For such a case as a roller chain drive for motorcycles, however, it is more reasonable to idealize it as a line source owing to its large aspect ratio. A semi-cylindrical hypothetical surface is therefore selected to surround the chain drive for sound pressure measurement and further for the calculation of chain drive sound power. As shown in Figure 8, a total of 18 microphone locations on a hypothetical surface are selected.

Denoting the sound pressure level at each designated point as $L_{pi}$, the average sound pressure level over the surrounding surface, $L_p$, can be calculated by using the following

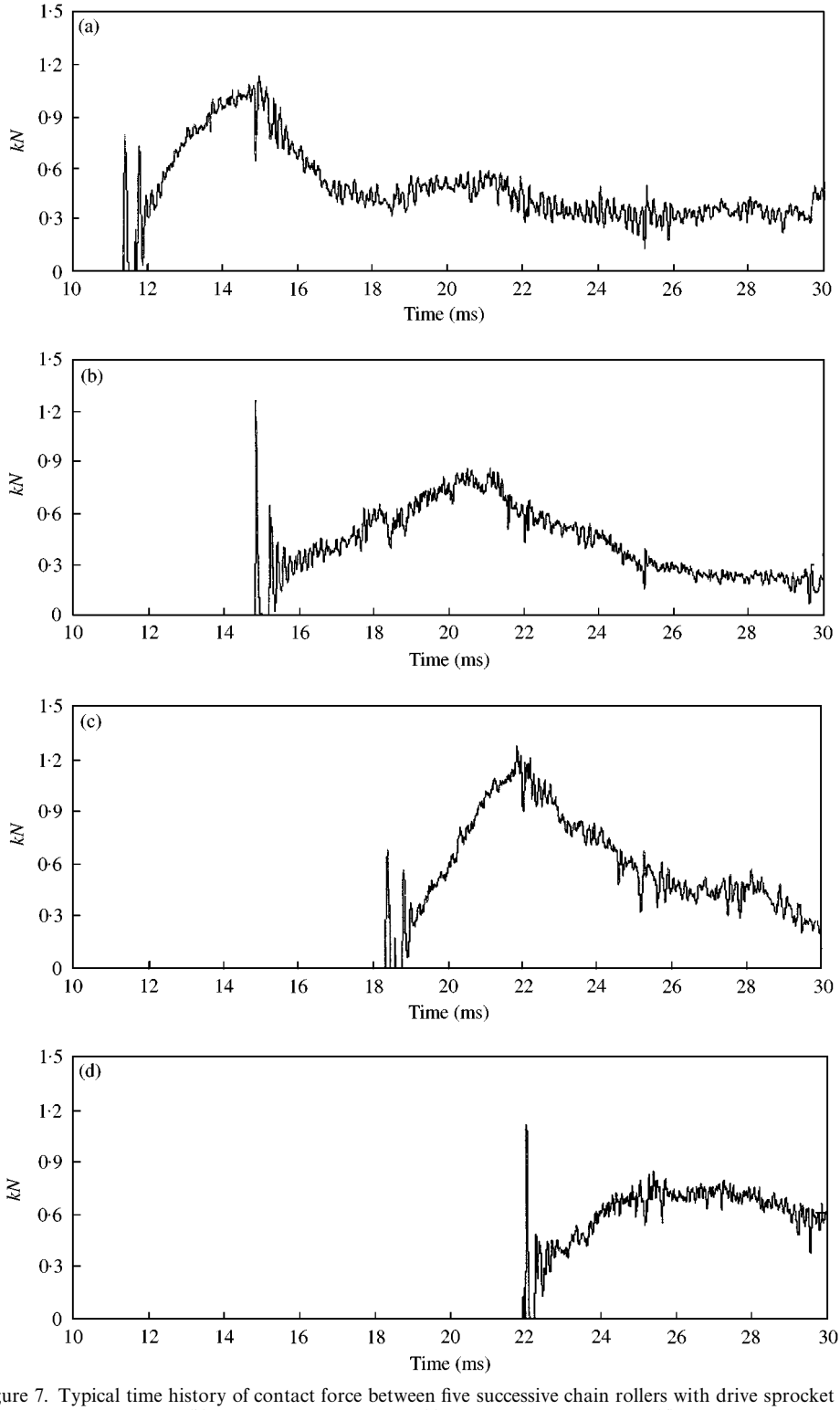


Figure 7. Typical time history of contact force between five successive chain rollers with drive sprocket teeth. (a) ——, Contact_Force_1; (b) ——, Contact_Force_2; (c) ——, Contact_Force_3; (d) ——, Contact_Force_4.

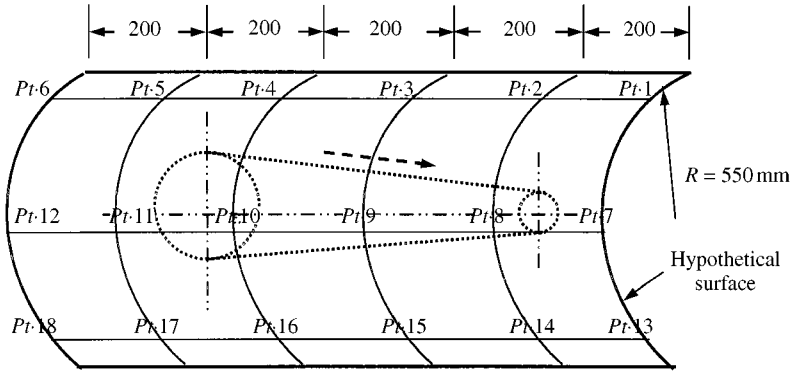


Figure 8. Microphone locations on a semi-cylindrical hypothetical surface surrounding the chain drive.

TABLE 4

*Comparison between prediction and experimental measurement (in dB)*

| Position | 1 | 2 | 3 | 4 | 5 | 6 |
|---|---|---|---|---|---|---|
| Measurement | 90·3 | 90·3 | 88·0 | 86·5 | 85·9 | 83·8 |
| Prediction | 89·0 | 89·3 | 87·8 | 85·9 | 84·0 | 81·9 |
| Position | 13 | 14 | 15 | 16 | 17 | 18 |
| Measurement | 88·6 | 87·5 | 86·9 | 85·3 | 84.3 | 83·7 |
| Prediction | 88·5 | 88·8 | 87·3 | 86·7 | 84·8 | 82·1 |

equation:

$$L_p = 10\log_{10}\left[1/N \sum_{i=1}^{N} 10^{0\cdot1L_{pi}}\right]. \tag{35}$$

According to the theoretical relation between the sound power and sound pressure of a line source in the free field, the sound power level may be further calculated from

$$L_W = L_p + 10\log_{10}(S/S_0), \tag{36}$$

where $S$ is the area of the hypothetical surrounding surface, $S = \pi RL$ for the measurement and $S = 2\pi RL$ for the prediction, and $S_0$ is the reference area, $S_0 = 1\ \mathrm{m}^2$.

A comparison between the measured noise levels and the predicted ones is given in Table 4 where the noise level at point #1–6 and #13–18 are tabulated. The data indicate that the predicted results of noise level of roller chain drive systems are in good agreement with measurements, especially at those locations close to the driving engagement point. The biggest sound pressure level difference between the prediction and measurement is about 2 dB. This is below the expectation, since the measurement is conducted in a semi-anechoic room but the prediction is made with an assumption of freefield radiation. The predicted sound power of the noise from the whole drive system is 93·3 dB, which is in good

agreement with the measurement, namely, 93·8 dB. The comparison illustrates that the reliability and the accuracy of the proposed approach and the numerical models are sufficient for the calculation of the meshing noise from roller chain drive systems.

From the data listed in Table 4, one can find that the noise levels at those locations closer to the engaging point of rollers with drive sprocket is much higher than those far away from this point. Comparing the sound pressure levels at point $\#2$ which is near the engaging point of rollers with drive sprocket and $\#14$ near the releasing point from the engagement, the difference of the measured sound pressure level is 2·8 dB. The result indicates that to the noise radiation from the whole system, the impact of the engaging rollers with the drive sprocket is more important than that with the driven sprocket. However, the prediction shows that the sound pressure level at point $\#2$ is only 0·5 dB higher than that at point $\#14$. This discrepancy with the measurement may be attributed to the fact that, in the theoretical acoustic model, the sound wave due to the roller/sprocket impact is assumed to propagate in a completely free environment. All the "barrier" effects of rollers and sprockets on the sound wave propagation from the impact point to other spatial points are ignored in the calculation. This can explain why the predicted sound pressure level at point $\#14$ (88·8 dB) is so high that it is comparable with the noise level at point $\#2$ (89·3). In the real situation, owing to the "barrier" effects of the moving rollers and rotating sprockets, the propagation of the sound wave due to the impact between rollers and drive sprocket (i.e., near point $\#2$) is attenuated largely when it reaches point $\#14$.

To clarify the relative importance of the impact of chain rollers with the drive and driven sprocket, "drive noise" and "driven noise" are adapted, respectively, representing the noise due to the impact of engaging rollers onto the drive (small) sprocket and the one due to the impact of engaging rollers onto the driven (big) sprocket. A comparison between drive and driven noise is shown in Table 5 where the calculated noise levels at 12 hypothetical locations are listed. It is clearly indicated that drive noise is much more important than driven noise to the noise radiation from the whole drive system. This is obviously attributed to the fact that the relative impact velocity of rollers onto the drive sprocket, owing to the higher rotating speed of the sprocket, is much higher than that of the rollers onto the driven sprocket. This sound power of drive noise is 90·0 dB, and that of driven noise is 84·1 dB, i.e., nearly 6 dB lower than the drive noise.

The acoustical energy of the noise from a chain drive system is the contribution of both the engaging rollers and vibrating sprockets under the excitation of impacts of the rollers onto the sprocket tooth. In all the above calculations, the noise radiation due to the surface vibration of two sprockets is assumed negligible considering its little contribution to the noise radiation by the whole drive system. Using Holmholtz surface integral theorem [21],

TABLE 5

*Comparison between drive and driven noise (in dB)*

| Position | 1 | 2 | 3 | 4 | 5 | 6 |
|---|---|---|---|---|---|---|
| Drive Noise | 88·8 | 89·1 | 87·1 | 84·2 | 81·4 | 78·8 |
| Driven Noise | 76·6 | 78·9 | 80·9 | 81·9 | 81·3 | 79·5 |
| Position | 13 | 14 | 15 | 16 | 17 | 18 |
| Drive Noise | 88·4 | 88·6 | 87·0 | 84·5 | 82·0 | 79·6 |
| Driven Noise | 75·1 | 78·3 | 81·6 | 83·4 | 82·3 | 79·2 |

the sound pressure levels of the noise radiated by the vibrating surfaces of the drive (small) sprocket and driven (big) sprocket with lighting holes are calculated in order to verify the reasonability of this assumption. The results are listed in Table 6 and compared with the drive and driven roller noise at a corresponding point. In the table, point A indicates a location coincident with the hypothetical point $\#2$ for the drive sprocket and $\#16$ for the driven sprocket. It can be easily seen that the contribution of both the drive and driven sprocket surfaces to the acoustical energy of the noise from the chain drive system is very small compared with the roller noise. For example, the noise level due to the vibrating surfaces of the driven sprocket with lighting holes is 74·4 dB at point $\#16$ while the driven rollers noise at the same point is 84·5 dB. According to the summation principle of decibel values, the total noise level of these two parts is 84·9 dB, which means that neglecting the contribution of the sprocket surface to the system noise would not significantly deteriorate the accuracy of our prediction model and approach. The lowest noise level by the drive (small) sprocket is attributed to its small area of radiating surface.

## 5. SUMMARY

An efficient and practical approach for the noise level prediction of roller chain drives is presented. An acoustical model, which relates the acceleration response of the chain drive components and generated sound is developed based on the acoustic field created by oscillating rigid cylinders. Finite element techniques and numerical software codes are employed to produce accelerations of the chain rollers. Using the information of numerical simulation of the impact of chain rollers onto the sprocket tooth, the sound pressure levels at different points located on a hypothetical cylindrical surface are calculated and further compared with existing experimental results. It is shown that the prediction is in good agreement with experimental measurements and the procedure works in a practical manner for the noise prediction of the complex chain drive systems.

Main concluding remarks on the impact noise of chain drive system can be drawn. First, owing to higher rotational speed of the drive (smaller diameter) sprocket for motorcycles and associated stronger impact between the engaging rollers on the tight side with the sprocket tooth, the sound pressure level of the drive noise is much higher than that of the driven noise. Second, the contribution of noise radiation from both drive and driven sprockets' surfaces to the acoustical energy of the noise from a chain drive system is so small compared with the roller noise that it can be neglected in the noise level prediction of roller chain drives for motorcycles. This will not deteriorate the accuracy significantly.

More importantly by integrating the presented approach into an existing computer-aided engineering (CAE) environment, a complete virtual acoustical simulation capability for chain drive design can be implemented and the noise level of the selected chain drive can be known in the design stage in a time- and cost-efficient manner.

TABLE 6

*Sound pressure level (SPL) of noise radiation from sprocket surfaces and comparison with drive and driven noise*

| Noise radiator | Drive sprocket | Drive noise | Driven sprocket | Driven noise |
|---|---|---|---|---|
| SPL (dB) at point A | 72·5 | 89·3 | 74·4 | 84·5 |

## REFERENCES


1. K. W. WANG and S. P. LIU 1991 *Shock and Vibration Digest* **23**, 8–13. On the noise and vibration of chain drive systems.
2. M. R. NAJI and K. M. MARSHEK 1983 *Mechanism and Machinery Theory* **18**, 349–356. Analysis of sprocket load distribution.
3. M. R. NAJI and K. M. MARSHEK 1984 *Mechanism and Machinery Theory* **19**, 197–203. Analysis of roller chain sprocket pressure angles.
4. J. C. CONWELL and G. E. JOHNSON 1995 *Mechanism and Machinery Theory* **31**, 533–544. Experimental investigation of link tension and roller–sprocket impact in roller chain drives.
5. M. S. KIM and G. E. JOHNSON 1992 *American Society of Mechanical Engineers International Power Transmission and Gearing Conference*, DE-Vol. 43-2, 689–702. Mechanics of roller chain–sprocket contact.
6. G. BOUILLON and G. V. TORDION 1965 *Journal of Engineering for Industry*, 243–250. On polygonal action in roller chain drives.
7. C. K. CHEN and F. FREUDENSTEIN 1988 *American Society of Mechanical Engineers Journal of Mechanisms, Transmission, and Automation in Design* **110**, 269–275. Toward a more exact kinematics of roller chain drives.
8. S. T. ARIARATNAM and S. F. ASOKANTHAN 1987 *Journal of Mechanism, Transmission, and Automation in Design* **109**, 412–418. Dynamic stability of chain drives.
9. S. MAHALINGAM 1957 *British Journal of Applied Physics* **8**, 45–148. Transverse vibrations of power transmission chains.
10. J. N. FAWCETT and S. W. NICOL 1979 *Fifth World Congress on Theory of Machines and Mechanisms*, 1482–1485. A theoretical investigation of the vibration of roller chain drives.
11. N. M. VEIKOS and F. FREUDENSTEIN 1992 *Mechanical Design and Synthesis American Society of Mechanical Engineers* DE-Vol. 46, 431–450. On the dynamics analysis of roller chain drives.
12. W. CHOI and G. E. JOHNSON 1993 *Vibrations of Mechanical Systems and the History of Mechanical Design American Society of Mechanical Engineers* DE-Vol. 63, 29–40. Vibration of roller chain drives at low, medium and high operating speeds.
13. M. S. KIM and G. E. JOHNSON 1993 *Advances in Design Automation American Society of Mechanical Engineers* DE-Vol. 65-1, 257–268. A general, multi-body dynamic model to predict the behavior of roller chain drives at moderate and high speeds.
14. K. UEHARA and T. NAKAJIMA 1979 *Fifth World Congress on Theory of Machines and Mechanisms*, 906–909. On the noise of roller chain drives.
15. W. A. STONR, M. W. TRETHEWEY and K. W. WANG 1990 119*th Meeting of the ASA* **98**, s 136. Experimental evaluation of chain noise.
16. S. P. LIU, K. W. WANG, S. I. HAYEK, M. W. TRETHEWEY and K. H. K. CHEN 1997 *Journal of Sound and Vibration* **203**, 41–62. A global-local integrated study of roller chain meshing dynamics.
17. P. K. BANERJEE and R. BUTTERFIELD 1981 *Boundary Element Methods in Engineering Science*. London: McGraw-Hill.
18. N. ATALLA and R. J. BERNHARD 1994 *Applied Acoustics* **43**, 271–294. Review of numerical solutions for low-frequency structural-acoustic problems.
19. M. CHOW 1985 *American Society of Mechanical Engineers Journal of Mechanism, Transmission, and Automation in Design* **107**, 123–130. Inertia effects of a roller-chain on impact intensity.
20. H. ZHENG and Z. XU 1998 *Technical Report, Centre for Computational Mechanics. The National University of Singapore*. Application of computational mechanics techniques for acoustic analysis of a chain–sprocket system.
21. A. D. PIERCE 1981 *Acoustics: An Introduction to Its Physical Principles and Applications*. New York: McGraw-Hill Book Company.
22. M. ABRAMOWITZ and I. A. STEGUN 1964 *Handbook of Mathematical Functions*. New York: Dover Publications, Inc.
23. Y. F. WANG and Z. F. TONG 1992 *Journal of Sound and Vibration* **159**, 295–303. Sound radiated from the impact of two cylinders.
24. K. P. QUEK, Y. NOGUCHI and T. ITO 1999 *Technical Report, SUNSTAR Engineering Inc., Japan*. Noise level measurement of chain drive with different driven sprocket.
25. International Organization for Standardization 1975 *Precision Methods for Anechoic and Semi-Anechoic Rooms*. ISO3745, Switzerland.